Negative photoconductance in a biased multiquantum well with filter barriers

Anibal T. Bezerra,[1,2,*] Marcelo Z. Maialle,[2,3] Marcos H. Degani,[2,3] Paulo F. Farinas,[1,2] and Nelson Studart[1,2]
[1]*Departamento de Física, Universidade Federal de São Carlos, 13565-905, São Carlos, SP, Brazil*
[2]*DISSE - Instituto Nacional de Ciência e Tecnologia de Nanodispositivos Semicondutores, CNPq/MCT, Brazil*
[3]*Faculdade de Ciências Aplicadas, Universidade Estadual de Campinas, 13484-350, Limeira, SP, Brazil*
(Received 15 August 2013; revised manuscript received 20 November 2013; published 3 January 2014)

In this paper the photon-assisted electron motion in a multiquantum well (MQW) semiconductor heterostructure in the presence of an electric field is investigated. The time-dependent Schrödinger equation is solved by using the split-operator technique to determine the photocurrent generated by the electron movement through the biased MQW system. An analysis of the energy shifts in the photocurrent spectra reveals interesting features coming from the contributions of localized and extended states on the MQW system. The photocurrent signal is found to increase for certain values of electric field, leading to the analog of the negative conductance in resonant tunneling diodes. The origin of this enhancement is traced to the mixing of localized states in the QWs with those in the continuum. This mixing appears as anticrossings between the localized and extended states and the enhanced photocurrent can be related to the dynamically induced Landau-Zener-Stückelberg-Majorana transition between two levels at the anticrossing.

DOI: 10.1103/PhysRevB.89.035301 PACS number(s): 73.21.−b, 73.63.Hs, 78.67.De

I. INTRODUCTION

It is well known that the application of external electric fields to quantum objects leads to intriguing phenomena like, among others, the quantum-confined Stark effect which describes the effect of an external electric field upon the optical spectrum of a quantum well (QW) [1]. Another striking phenomenon is the carrier localization in the single miniband of a superlattice under strong electric field, the Wanier-Stark ladder [2–4]. Nowadays, fueled by technological innovation, old physical concepts and phenomena found in semiconductor heterostructures have been revived and broad avenues are still open for designing new devices ranging from quantum cascades lasers [5,6], and, for the sake of our interest, to the infrared (IR) photodetectors based on intrasubband tunneling between states localized in quantum wells [7–10] or/and quantum dots (QD) [11–15], and superlattices [16–18]. Even though most of these devices are now commercially available, there are presently a lot of unresolved questions concerning the optimal design and even the basic physical mechanisms underlying the behavior of these systems. Laterally, the gradual improvement of computational approaches has been yielding investigations of, e.g., out-of-equilibrium transport of charge and nonlinear phenomena such as the role of multiple-photon absorptions [19].

In the present paper a theoretical approach based on a simple model suited for charge transport calculations is adopted in the investigation of a structure composed by alternating wells and barriers generating a multiple quantum well (MQW) profile, under the simultaneous application of static and oscillating biases. The proposed structure has additional barriers inside the QW barriers, whose potential confinement exceeds the QW ones, generating a superlatticelike potential profile above the wells (for more details, see Sec. II). Given the length scales of the quantum wells analyzed (in the tenths of nanometer range) the classical oscillating field produces the same effects, from the computational perspective, as if fully quantized photon fields were used. Hence, the oscillating electric field can be viewed either as a laser beam, given the frequencies chosen, in the THz domain, or as a very fast-oscillating alternated field, driving the structure out of equilibrium. We work within the latter view but adopt the former view by calling the resulting charge motion throughout the structure by "photocurrent."

The photocurrent generated is shown as emerging from simple (yet usual) model assumptions. As expected, a series of resonances appear in the plot of photocurrent versus photon energy whose peaks are understood in terms of the contributions of each individual quantum well to the photocurrent. Stark shifts of these resonances are described in terms of the electronic states involved in the photocurrent generation, and a detailed analysis reveals the role of the localized and extended states. Among the features observed in the photocurrent spectra is the generation of reverse (against bias)[20] photocurrents for certain photon wavelengths and low enough biases, which are known to appear in measurements. The resonant photocurrent signal shows an interesting dependence on the applied electric fields, namely an enhanced photocurrent signal for certain values of field, leading to a behavior which resembles the negative-conductance phenomenon known in resonant tunneling diodes [21,22]. The origin of this enhancement is traced to the mixing of localized states in the MQW structure with the extended states in the energy continuum. This mixing appears as anticrossings between the localized and extended states such that the enhanced photocurrent can be related to the Landau-Zener-Stückelberg-Majorana (LZSM) transition [23–26], that is, a transition dynamically induced between two levels at an anticrossing [27,28].

II. MULTIPLE QUANTUM WELL SYSTEM AND THEORY

Our MQW structure illustrated in Fig. 1(a) is formed by ten GaAs QWs of 5 nm thickness and $Al_{0.15}Ga_{0.85}As$ barriers of 11 nm. Inside each barrier of the MQW we place thin $Al_{0.30}Ga_{0.70}As$ filter barriers of 3 nm, generating a superlatticelike potential profile above the wells. This profile

*anibal@df.ufscar.br

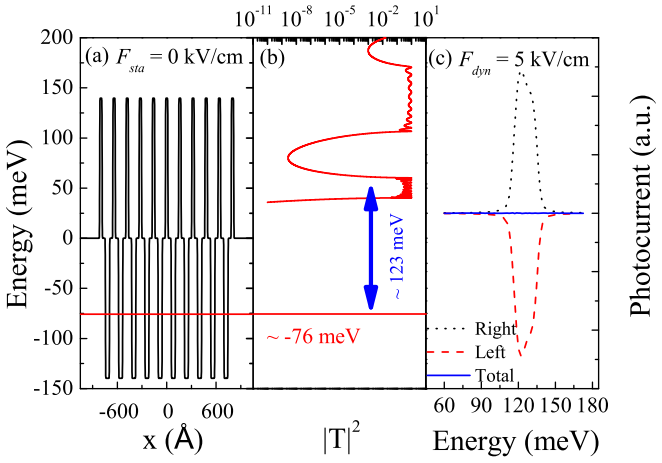

FIG. 1. (Color online) (a) Potential profile of the structure composed by alternating wells and barriers generating a multiple quantum well profile. The additional potential barriers inside the QW barriers generate a superlatticelike potential profile above the wells contributing for the formation of the minibands shown in (b). (b) Transmission coefficient through the structure, showing the minibands MB1 and MB2. (c) Photocurrent for zero electric field. The black-dotted (red-dashed) line represents the right (left) component of the photocurrent, and the blue line represents the total photocurrent.

is conceived to create localized states in the MQW continuum in such a way that their coupling to the system ground state is increased, while keeping them sufficiently extended to warrant generation of photocurrent. The system is designed to have, in the absence of external biases, 10 very narrow spaced levels around −76 meV inside the MQW and a series of minibands in the continuum region above the QWs. As we can see in Fig. 1(b) the lowest miniband (MB1) is around +47 meV.

Figure 1(b) shows the transmission coefficient for our structure for zero electric field. The minibands have ten distinguishable peaks, in correspondence to the ten wells of the MQW. We can observe that the energy separation between the bound states in the QWs and the center of the MB1 is approximately 123 meV, which agrees very well with the photocurrent peak shown in Fig. 1(c). As a consequence of the structure symmetry, the net photocurrent is zero, at zero electric field, where the contributions of right and left current peaks cancel out. From these individual peaks, one electron is photoexcited from the QW bound state to the first miniband by a photon of ∼123 meV and escapes from the filter barriers region to contribute to the photocurrent signal.

The electron excitation from the bound states in the QW is provided by the application of an oscillating electric field perpendicular to the heterostructure layers. Also a static electric field is applied in the same direction of the oscillating field. The Hamiltonian of the electron in the effective-mass approximation is hence given by

$$\widehat{H} = -\frac{\hbar^2}{2m^*}\frac{d^2}{dx^2} + V(x) - ex[F_{\rm sta} - F_{\rm dyn}\sin(\Omega t)], \quad (1)$$

which is the one-dimensional part of the full Hamiltonian with the usual assumptions of conservation of the momentum parallel to the layers. $V(x)$ is the profile potential of the structure sketched in Fig. 1(a), m^* is the electron effective mass considered uniform throughout the system, and e is the electron charge. In Eq. (1), $F_{\rm dyn}$ and $F_{\rm sta}$ are the intensity of the oscillating and static field, respectively.

We use a numerical approach to determine the time evolution of the wave functions given by

$$\Psi(x,t+\Delta t) = e^{-i\widehat{H}\Delta t/\hbar}\Psi(x,t), \quad (2)$$

where Δt is the time increment, $\hbar$ is the reduced Planck constant, and $\widehat{H}$ is the system Hamiltonian within the effective-mass approximation, given by Eq. (1). Since the kinetic operator $\widehat{T}$ and potential operator $\widehat{V}$ in the Hamiltonian do not commutate, the exponential operator on Eq. (2) cannot be performed exactly and some approximations need to be used. In the present work we have used the split-operator technique [19]

$$e^{-i(\widehat{T}+\widehat{V})\Delta t/\hbar} = e^{-i\widehat{V}\Delta t/2\hbar}e^{-i\widehat{T}\Delta t/\hbar}e^{-i\widehat{V}\Delta t/2\hbar} + O(\Delta t^3).$$

Thus, successive applications of this time-evolution operator evolve the initial wave function from $t = 0$ to $t > 0$, within an error of the order of Δt^3. If this procedure is realized in imaginary time, making $t \to -i\tau$ and setting $F_{\rm dyn} = 0$, we can calculate the eigenstates and eigenenergies of the MQW structure as a function of the electric field [19]. For the present method we used hard walls as boundary conditions, i.e., the wave function vanishes at the boundaries. To avoid reflections of the wave functions at the boundaries, we implemented exponential imaginary absorber barriers on the potential at large distances from the system's active region [29].

The particle current flowing toward both sides of the system can be computed as

$$J_c(t) = \Re\left[\frac{\hbar}{im^*}\Psi(x,t)^*\frac{\partial\Psi(x,t)}{\partial x}\right]_{x=x_c}, \quad (3)$$

where $\Psi(x,t)$ is the system wave function under the oscillating electric field and the index $c = left$ or $c = right$ represents the left and right components of the photocurrent [Fig. 1(c)]. The current J_c is then integrated over time to obtain

$$I = \frac{e}{T_p}\int_0^{T_p}[J_{right}(t) - J_{left}(t)]dt, \quad (4)$$

where T_p is an upper bound time which depends on the frequency of the oscillating field. A detailed discussion of this technical point is made in Ref. [29]. The net photocurrent is given by the sum of the photocurrents generated by initial states localized in each QW. In what follows, ohmic effects are not taken into account and the photocurrent is purely coherent.

III. RESULTS AND DISCUSSION

Hereafter we number orderly the QWs [shown in Fig. 1(a)] from the right-hand side to the left-hand side by 1st QW up to 10th QW. As expected, when the structure is biased the energy level of the 1st QW is lowered relative to the 10th QW due to the Wannier-Stark effect [2,30].

In Fig. 2 the dependence of the photocurrent with the electric field is depicted for $T_p = 1$ ps and $F_{\rm dyn} = 5$ kV cm^{-1}. Due to the breaking of the potential symmetry, the states became localized with an energy shift of $\Delta E = edF_{\rm sta}$, where d is the period of the structure. As shown in the inset of Fig. 2,

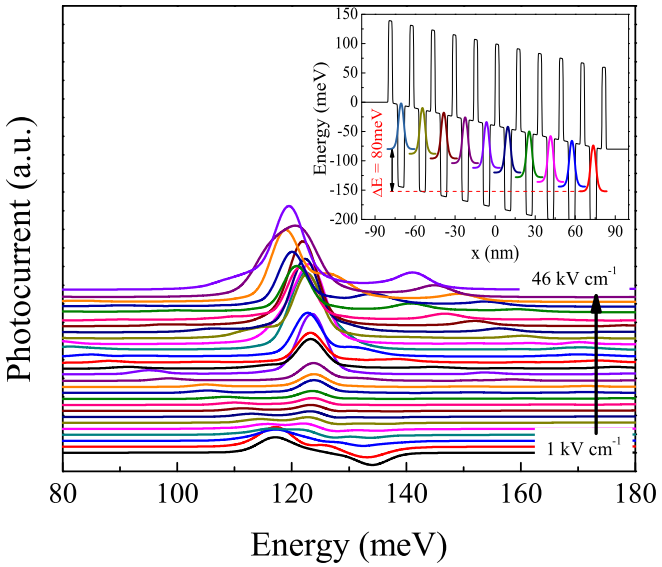

FIG. 2. (Color online) Photocurrent spectra for different applied electric fields. Curves are vertically shifted for better visualization. The inset shows the potential profile and the ground state wave function localized in each well for a 5 kV cm^{-1} electric field. We observe that the localized states spread over a energy region of $\Delta E \simeq$ 80 meV. As a rule of thumb the regions where the photocurrents are constant (straight horizontal lines) can be taken as the zero-value baseline for a vertical scale (note that some values of the photocurrent are thus negative).

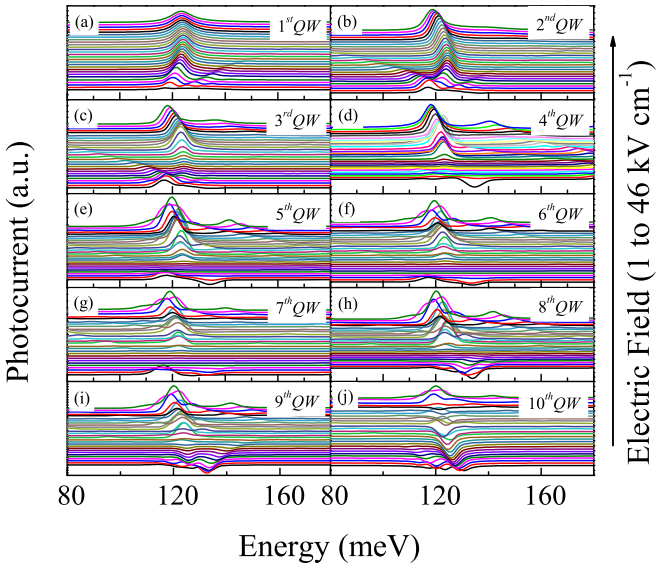

FIG. 3. (Color online) Photocurrent spectra for different electric fields ranging from 1 to 46 kV cm^{-1}. The panels (a)–(j) are related to the photocurrent of each individual QW (1st to 10th), respectively. Curves were vertically shifted for better visualization, and different scales are used in each graph. As a rule of thumb the regions where the photocurrents are constant (straight horizontal lines) can be taken as the zero-value baseline for a vertical scale (note that some values of the photocurrent are thus negative).

we clearly observe the effect of the Wannier-Stark localization as the states spread over an 80 meV energy region for an electric field of 5 kV cm^{-1}. The same occurs with the miniband states in the continuum.

In order to better understand the total photocurrent spectra in Fig. 2 we look separately to each QW photocurrent contribution as shown in Fig. 3. We noticed (not shown here) that for low and high bias regimes, the major contribution to the total photocurrent comes from the more external QWs, that is, mostly from the first two QW on the right-hand side and the last two on the opposite side. Then it is enough for clear understanding to focus our discussion on the mentioned QWs.

In Fig. 3(a), which represents the photocurrent of the 1st QW, we can see for low biases two positive peaks. Both peaks blueshift with increasing of the electric field, and the Wannier-Stark relationship $\Delta E = ed F_{\text{sta}}$ is approximately obeyed. We associate the main photocurrent peak in Fig. 3(a) to the transition from the ground state of the 1st QW to the lowest state of the first miniband (MB1) located in the filter barriers region. Both states are spatially localized in the 1st QW region, therefore enhancing the overlap of the wave functions that favors the transition and, consequently, the photocurrent signal. For simplicity, even in the cases for which there is localization we will use the term "miniband" in reference to these states. The second photocurrent peak seen in Fig. 3(a) is related to the transition between the 1st QW bound state and the second lowest-energy state of the MB1 which is spatially localized in a neighboring 2nd QW. In this case, the relative energy shift between these states in the presence of bias signals the Stark ladder formation [4]. As the delocalized states of the miniband state becomes localized in the 2nd QW, the overlap with the 1st QW bound state decreases, resulting in the observed decrease of the second peak. A similar argument is valid for the photocurrent contribution of the 2nd QW and shown in Fig. 3(b).

We now discuss the contributions to the overall photocurrent of the 9th QW and 10th QW in the left-hand side of the MQW structure with filter barriers. As we can see in Figs. 3(i) and 3(j), the photocurrent contribution of these QWs presents negative values (i.e., current flowing against the electric field) for low bias which become positive with increasing of the electric field. This phenomenon was already demonstrated and well discussed by Sirtori and collaborators [20], and is related to the transition between the ground state and the higher energy states of MB1 which are extended over the left-hand side of the MQW structure allowing the electrons to conduct against the electric field direction. By further increasing the electric field the whole structure becomes transparent to the photoexcited electrons favoring the action of the electric field in producing positive photocurrent. The shifts in the peak positions and the decrease in the peak intensities are also related to Stark ladder formation and to the decrease of the overlap between wave functions of different QWs, respectively.

Looking more carefully to the photocurrent dependence on bias, we see in Fig. 4 (same results as Fig. 2 in a different glance) that the intensity of the main peak at about 120 meV first decreases, but then starts to increase for certain electric field values. The origin of the first decrease observed for intermediate biases is the Stark shifts of the positive and negative peaks, already discussed in Figs. 3(a) and 3(j), respectively. We again call to attention, from these figures,

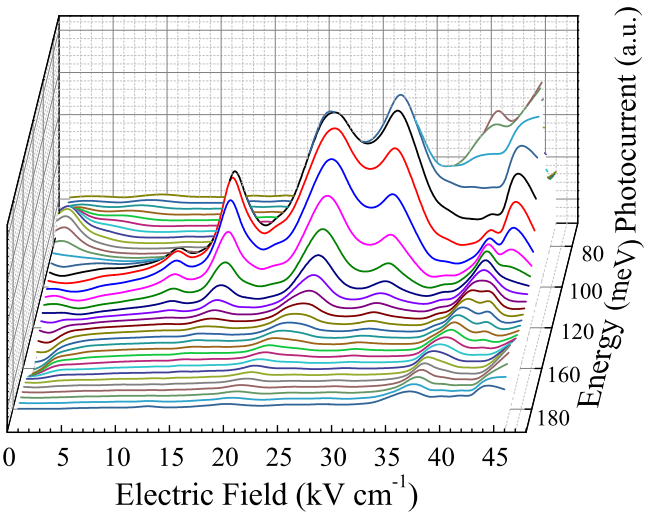

FIG. 4. (Color online) Photocurrent is depicted as a function of the electric field and the energy showing the peaks shifts discussed in the text.

that the positive peak slightly blueshifts while the negative one redshifts with a bias increase. As an expected consequence, in the intermediate bias region the peaks' intensities partially cancel out each other contributing to diminish the total photocurrent.

The photocurrent enhancement seen in Fig. 4 for certain electric fields has a different origin around the excitation energy 120 meV, namely the mixing between extended and localized states. Because we construct our system placing a thinner filter barrier inside each barrier of the MQW structure which led to the formation of very close quasicontinuum states (minibandlike, as we call them earlier) and still enough localized in the QWs region, we achieve a bias dependent coupling of the QW ground states and the extended states in the continuum (above the MQW structure). In order to make clear this state coupling, we present in Fig. 5(a) the MQW energy spectrum as a function of the electric field. For increasing bias the miniband states Stark shift and many crossings are seen. In Figs. 5(b) and 5(c) we focus on the region of the energy spectrum given by the red circle in Fig. 5(a), in which the anticrossing between the first and second minibands is clearly depicted. The dot sizes in Fig. 5(b) are proportional to the participation ratio,

$$P = \frac{1}{L}\frac{\left(\int |\Psi(x)|^2 dx\right)^2}{\int |\Psi(x)|^4 dx},$$

where the integration is over the entire space, L is the size of the system, and the numerator will be one for states normalized to unity. P, as introduced by Bell and Dean [31] and also described by other authors [32,33], is basically a measure of how extended is the state, in other words, extended states have larger P. As we can observe in Fig. 5(b), the crossing occurs between an initially localized state of the MB1, with smaller P (solid gray dotted curve) and an initially extended state of the MB2, with greater P (open brown dotted curve). During the crossing, both states have comparable participation ratio,

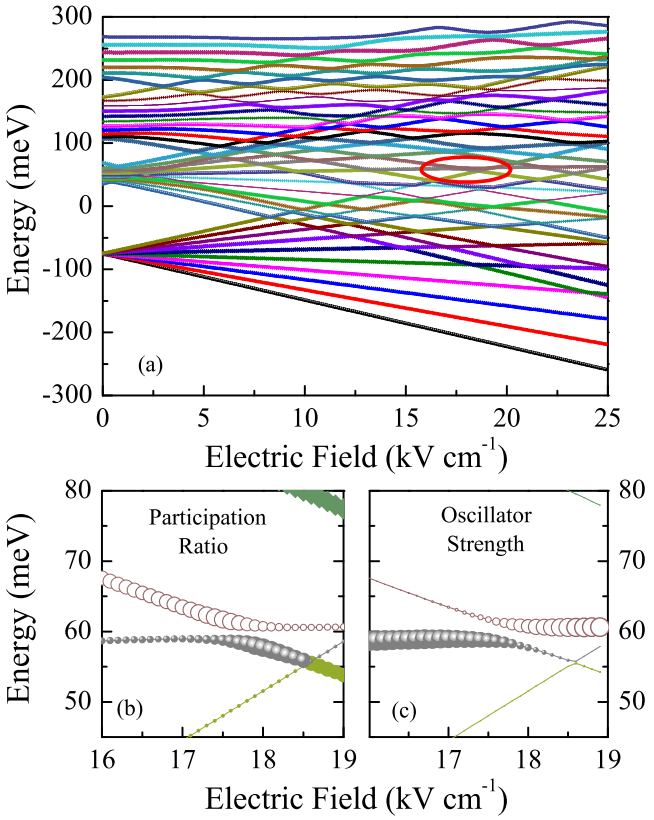

FIG. 5. (Color online) (a) Energy spectrum as a function of the electric field. (b) Zooming of the encircled region of the energy spectrum of (a) showing the levels anticrossing. The dot sizes are proportional to the participation ratio which means the larger the dot the more the state is delocalized. (c) Same as (b) with the dot sizes proportional to the oscillator strength.

changing their character after the crossing. Namely, the former becomes extended and the latter becomes localized.

In Fig. 5(c), the dot sizes are proportional to the oscillator strength (f_{if}), defined as

$$f_{if} = \frac{2m^*}{\hbar^2}(E_i - E_f)|\langle\Psi_i(x)|x|\Psi_f(x)\rangle|^2,$$

where E_i and E_f are the eigenvalues of the initial $\Psi_i(x)$ and final $\Psi_f(x)$ states of the transition, respectively. As we can observe, the localized state has a greater oscillator strength than the extended one. In the anticrossing we have a particular situation in which both the states can be excited, since they have reasonable oscillator strength, and they are sufficiently extended states (large P), allowing for current generation. Therefore the mixing of localized and extended states in the anticrossing regions are the origin to the photocurrent enhancement seen in Fig. 4. The phenomenon could be related to the LZSM problem [23–26,34], namely, a dynamical induced transition between states with energy levels in an anticrossing condition [35]. In this picture, the electron can be easily driven out from the filter barrier region only when the localized-extended mixing of states occurs, leading to peaks in the photocurrent $I(V)$ curves. For semiconductor superlattices similar features are observed in the current-voltage characteristics and related to the resonant character

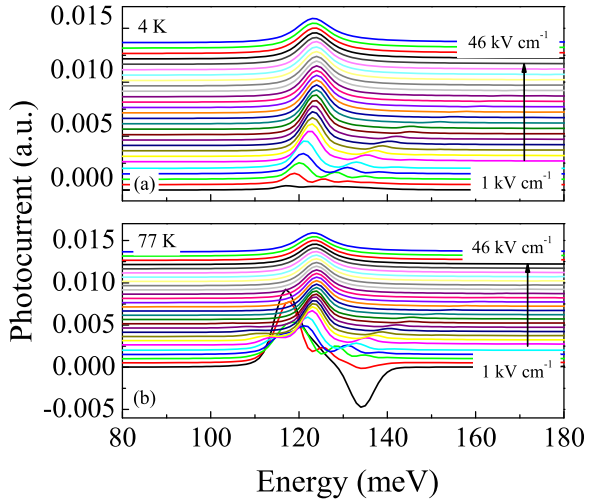

FIG. 6. (Color online) Photocurrent spectra for different electric fields, ranging from 1 to 46 kV cm^{-1}, using the Boltzmann factor to simulate temperature effects for (a) 4 K and (b) 77 K.

of the tunneling [36,37]. Different from previous works, the resulting effect in our system can be seen as the phenomenon of dynamic negative differential conductance, since Fig. 4 allows us to foresee a decrease in the (photo)current for specific electric field regions.

Finally, as our method does not take into account temperature effects, we use a multiplicative Boltzmann factor in the calculation of the photocurrent to give us a qualitative understanding of the temperature influence on the MQW system. We stress that there is no doping in our model system, yet there will be a source to charge carriers in a real system. The effect of the temperature considered here concerns only the redistribution of these carriers throughout the energy levels. The photocurrent will thus be given by

$$I(T) \propto \sum_{QW} e^{-\frac{E_{QW}}{k_B T}} I_{QW}, \tag{5}$$

where the sum runs over all the quantum wells, k_B is the Boltzmann constant, T is the temperature, and I_{QW} is the photocurrent contribution calculated from a single QW. The energies E_{QW} are measured always from the lowest energy present in the structure, which in the case illustrated in the inset of Fig. 2 corresponds to the energy of the 1st QW on the right, whose energy is taken to be zero.

Figure 6(a) shows the temperature dependent photocurrent $I(T)$ obtained with this approach as a function of the photon energy, for static electric fields varying from 1 to 46 kV cm^{-1} and $T = 4$ K. We note that the behavior of the T-dependent photocurrent is almost the same as the photocurrent calculated from the single QW (the 1st on the right) shown in the inset of Fig. 2 and whose results are depicted in Fig. 3(a). This can be understood from the exponential Boltzmann occupation factor that, for lower temperatures, tend to be negligible for states other than the lowest energy one, which is also more localized around its corresponding QW.

As the temperature is increased, the more energetic and delocalized levels become occupied. Figure 6(b) shows the photocurrent spectra at $T = 77$ K, a temperature that yields contributions from electrons that occupy the entire structure. For low biases the spectra are quite similar to the zero temperature limit. However by increasing the electric field the Stark shift triggers the effect of the Boltzmann factor, and as a result the negative-photoconductance phenomenon effect discussed earlier is quenched.

IV. CONCLUSIONS

In summary, we study the influence of an electric field provided by an external bias on the photocurrent generated in a semiconductor heterostructure that consists of multiple quantum wells with filter barriers. Generally speaking, the main photocurrent peak is weakly Stark shifted since this peak is dominated by the transition between the bound state of a single quantum well (QW) and states in a minibandlike group formed in the lowest energy region of the continuum, in the same position of the QW. Peaks that are strongly shifted are related to transitions between a QW bound state and miniband states of neighboring QWs. These peaks have intensities strongly dependent on the bias electric field due to spatial overlapping of the wave functions induced by the Wannier-Stark localization.

More importantly, we find a negative photoconductance, i.e., a decrease of the photocurrent with increasing of the electric field, whose origin is in the state mixing of localized and extended states. The former are excited states belonging to the miniband created by the filter barriers. The mixing is very sensitive to the bias, and the anticrossings of energy levels lead to Landau-Zener-Stückelberg-Majorana [23–26] transitions to extended states. Reference [38]; has experimentally found negative differential velocities in biased superlattices, however the observed resonances are claimed to be related to interband excitonic processes. In contrast, our calculations suggest the possibility for observation of negative differential conductance that is the result of localized-extended mixing of intraband electronic states, within the conduction band.

Finally, in order to simulate temperature effects we averaged the photocurrent over the quantum wells using a Boltzmann factor, with the expected result that lower energy quantum wells become increasingly more important for the net photocurrent signal as the temperature is lowered. We believe this simple way of including a Boltzmann factor and averaging over the quantum wells give us a qualitative estimate for the temperature behavior of the photocurrents.

ACKNOWLEDGMENTS

The authors are funded by DISSE-Instituto Nacional de Ciência e Tecnologia de Nanodispositivos Semicondutores and Conselho Nacional de Desenvolvimento Científico e Tecnológico (CNPq). M.H.D. and M.Z.M. acknowledge financial support from Fundação de Amparo à Pesquisa do Estado de São Paulo (FAPESP).

[1] D. A. B. Miller, D. S. Chemla, T. C. Damen, A. C. Gossard, W. Wiegmann, T. H. Wood, and C. A. Burrus, Phys. Rev. Lett. **53**, 2173 (1984).

[2] E. E. Mendez, F. Agulló-Rueda, and J. M. Hong, Phys. Rev. Lett. **60**, 2426 (1988).

[3] L. A. Cury and N. Studart, Superlatticces and Microstructures **3**, 175 (1987).

[4] M. H. Degani, Appl. Phys. Lett. **59**, 57 (1991).

[5] J. Faist, F. Capasso, C. Sirtori, D. L. Sivco, J. N. Baillargeon, A. L. Hutchinson, S. G. Chu, and A. Y. Cho, Appl. Phys. Lett. **68**, 3680 (1996).

[6] C. Gmachl, F. Capasso, E. E. Narimanov, J. U. Nockel, A. D. Stone, J. Faist, D. L. Sivco, and A. Y. Cho, Science **280**, 1556 (1998).

[7] For a review, see B. F. Levine, J. Appl. Phys. **74**, R1 (1993).

[8] H. Drexler, J. S. Scott, S. J. Allen, K. L. Campman, and A. C. Gossard, Appl. Phys. Lett. **67**, 2816 (1995).

[9] S. D. Ganichev, E. Ziemann, Th. Gleim, W. Prettl, I. N. Yassievich, V. I. Perel, I. Wilke, and E. E. Haller, Phys. Rev. Lett. **80**, 2409 (1998).

[10] M. H. Degani, M. Z. Maialle, P. F. Farinas, and N. Studart, J. Appl. Phys. **110**, 104313 (2011).

[11] H. Lim, W. Zhang, S. Tsao, T. Sills, J. Szafraniec, K. Mi, B. Movaghar, and M. Razeghi, Phys. Rev. B **72**, 085332 (2005).

[12] P. L. Souza, A. J. Lopes, T. Gebhard, K. Unterrainer, M. P. Pires, J. M. Vilas-Boas, P. S. S. Guimar£es, G. S. Vieira, and N. Studart, Appl. Phys. Lett. **90**, 173510 (2008).

[13] M. H. Degani, M. Z. Maialle, P. F. Farinas, N. Studart, M. P. Pires, and P. L. Souza, J. Appl. Phys. **109**, 064510 (2011).

[14] D. R. Alvarenga, C. A. Parra-Murillo, R. M. S. Kawabata, P. S. S. Guimaraes, K. Unterrainer, M. P. Pires, G. S. Vieira, J. M. Villas-Boas, M. Z. Maialle, M. H. Degani, P. F. Farinas, N. Studart, and P. L. Souza, IEEE J. Quantum Electron. **48**, 1360 (2012).

[15] J. O. Kim, S. Sengupta, A. V. Barve, Y. D. Sharma, S. Adhikary, S. J. Lee, S. K. Noh, M. S. Allen, J. W. Allen, S. Chakrabarti, and S. Krishna, Appl. Phys. Lett. **102**, 011131 (2013).

[16] B. J. Keay, S. J. Allen, Jr., J. Galán, J. P. Kaminski, K. L. Campman, A. C. Gossard, U. Bhattacharya, and M. J. M. Rodwell, Phys. Rev. Lett. **75**, 4098 (1995).

[17] S. Zeuner, S. J. Allen, K. D. Maranovski, and A. C. Gossard, Appl. Phys. Lett. **69**, 2689 (1996).

[18] S. Zeuner, B. J. Keay, S. J. Allen, K. D. Maranowski, A. C. Gossard, U. Bhattacharya, and M. J. W. Rodwell, Phys. Rev. B **53**, R1717 (1996).

[19] M. H. Degani and M. Z. Maialle, J. Comput. Theor. Nanosci. **7**, 454 (2010).

[20] C. Sirtori, J. Faist, F. Capasso, D. L. Sivco, and A. Y. Cho, Appl. Phys. Lett. **63**, 2670 (1993).

[21] L. L. Chang, L. Esaki, and R. Tsu, Appl. Phys. Lett. **24**, 593 (1974).

[22] T. C. L. G. Sollner, W. D. Goodhue, P. E. Tannenwald, C. D. Parker, and D. D. Peck, Appl. Phys. Lett. **43**, 588 (1983).

[23] L. D. Landau, Phys. Z. Sowjetunion **2**, 46 (1932).

[24] C. Zener, Proc. R. Soc. A **137**, 696 (1932).

[25] E. C. G. Stückelberg, Helv. Phys. Acta **5**, 369 (1932).

[26] E. Majorana, Nuovo Cimento **9**, 43 (1932).

[27] H. Ribeiro, G. Burkard, J. R. Petta, H. Lu, and A. C. Gossard, Phys. Rev. Lett. **110**, 086804 (2013).

[28] H. Ribeiro, J. R. Petta, and G. Burkard, Phys. Rev. B **87**, 235318 (2013).

[29] M. Z. Maialle and M. H. Degani, Phys. Rev. B **83**, 155308 (2011).

[30] J. Bleuse, G. Bastard, and P. Voisin, Phys. Rev. Lett. **60**, 220 (1988).

[31] R. J. Bell and P. Dean, Dicuss. Faraday Soc. **50**, 55 (1970).

[32] H. Aoki, J. Phys. C **16**, L205 (1983).

[33] J. T. Edwards and D. J. Thouless, J. Phys. C **5**, 807 (1972).

[34] Y. Kayanuma and K. Saito, Phys. Rev. A **77**, 010101(R) (2008).

[35] G. Sun, X. Wen, B. Mao, J. Chen, Y. Yu, P. Wu, and S. Han, Nat. Commun. **1**, 51 (2010).

[36] J. R. Petta, H. Lu, and A. C. Gossard, Science **327**, 669 (2010).

[37] A. A. Andronov, E. P. Dodin, D. I. Zinchenko, and Yu. N. Nozdrin, Semiconductors **43**, 236 (2009).

[38] A. Sibille, J. F. Palmier, and F. Mollot, Appl. Phys. Lett. **60**, 457 (1992).